Analysis of a Novel Micro-Structured Regenerator Filler

A. Ghavami[1], C. Kirkconnell[2], S.M. Ghiaasiaan[1], W. Chen[3], M. Zagarola[3]

[1]Georgia Institute of Technology, Atlanta, GA 30332, USA
[2]West Coast Solutions, Huntington Beach, CA 92648, USA
[3]Creare LLC, Hanover, NH 03755, USA

ABSTRACT

Future progress with respect to improvement in the efficiency of PTRs depends on the development of a new regenerator filler material that can provide low hydrodynamic resistance, low thermal conduction in the main flow direction, and most importantly high thermal capacity at low temperatures. In this paper a CFD study is performed on a novel, non-rare-earth micro structured regenerator filler (Creare Microchannel Regenerator, CMR) that is under develop ment. CMR is a microfabricated, multi-layer structure and provides a complex flow passage for the working fluid. Pore-level CFD analysis is performed by defining and finely nodalizing peri odically repeating unit cells. The pore-level CFD-based study leads to the development of em pirical correlations for friction factor, as well as heat transfer coefficient between the regenerator filler structure and the working fluid. The validity of the results of the pore-level study is verified by CFD simulations where large segments of an entire regenerator consisting of a large number of unit cells are modeled.

INTRODUCTION

The regenerator is a key component of any Stirling or pulse-tube cryocooler. While playing a crucial role in rendering a positive heat lift possible, the inefficiency of the regenerator is also often the main cause of losses in a cryocooler. An ideal regenerator is a porous structure that has a low friction factor, low thermal conductivity in the main flow direction, and high thermal capacity. These requirements pose a challenge, in particular for small size cryocoolers in which high performance is crucial.

While linear cryocoolers in general benefit from reduced pressure drop and high Nusselt number in the heat exchanger components, microstructured regenerators such as the CMR are of particular interest in small, high frequency (say, >100 Hz) cryocoolers. These miniature cryo coolers often feature high internal flow velocities arising from small cross sectional flow areas, and because small size is at a premium, increasing the flow areas to mitigate the problem is not generally permissible. Traditional random and pseudo-random matrices, such as stacked screens, packed sphere beds, and packed fibers, yield intolerably high pressure drop losses, thus motivat ing a microstructured approach to mimic parallel plates or parallel tubes, which are inherently lower in flow resistance.

Cryocoolers 20, edited by S.D. Miller, R.G. Ross, Jr. and J.R. Raab

A novel, microstructured and synthetic regenerator filler has been under development at Creare, Inc. that can offer an excellent overall performance. Stirling and pulse tube cryocoolers are currently under development in which this microstructured regenerator filler will be utilized. In this paper we report on a methodology for deriving friction factor and solid-fluid heat transfer correlations for the aforementioned microstructured regenerator filler using pore-scale CFD simulations.

PHYSICAL SYSTEM

The regenerator core consists of a stack of thin disks with low thermal conductivity. The disks have long and slender involute slots. The longitudinal centerline of a slot thus makes an angle with the disk radius (i.e., a line drawn from the disk center to the location of interest), θ, that varies along the slot (see Fig 1). This angle will be referred to as the crossing angle. Pairs of disks with slots in opposite directions are stacked. These plates thus come together in opposite direction to make the involute geometry and porous medium as noted in the paired disk that is shown in Figure 1. The stacked disks thus form a porous annular flow passage where the pore-level flow passages have a hydraulic diameter equal to about 30 μm.

Operational conditions and scaled dimensions are summarized in Table 1. The outer diameter of the disk is used as the reference length for scaling. The regenerator is made of a polymer with low thermal conductivity and the working fluid is Helium. Temperature dependent properties are used for this study.

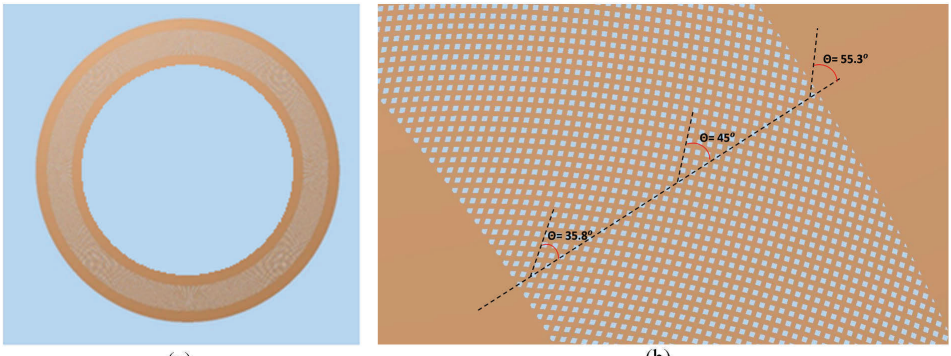

Figure 1. A pair disk of regenerator (a) the disk in its entirety, (b) zoom on the annulus section

Table 1. Operation conditions and dimensions of the regenerator; scaled dimensions are normalized with the disk outer diameter.

Hot end temperature (K)	300
Cold end temperature (K)	80
Mean pressure (MPa)	3.87
Reynolds number range	2-18
Scaled inner diameter of annulus	0.762
Scaled outer diameter of annulus	0.927
Scaled outer diameter of disk	1
Scaled thickness of each disk	4.013e-3
Scaled total regenerator length	1.975
Number of required pared disks	246
Scaled thickness of each slot	1.185e-3
Porosity of annulus	0.5
θ near the inner radii of annulus (degree)	35.8

UNIT CELLS AND DISK SLICE

All simulations were performed using Fluent 14.5 [1]. In view of the geometric complexity of the pore-level flow passages, evidently a rigorous and accurate definition of unit cells is a critical step. Furthermore, due to geometry complexity and variability of unit cells in both radial and axial directions, pore-level simulation of the entire regenerator will require too much computation and is impractical.

Two approaches are thus adopted. First, single unit cells are extensively simulated using appropriately fine nodalization, and the results are used for the development of empirical correlations. Second, an approximately 9° slice of an entire disk is simulated using a fine nodalization similar to the nodalization used for single unit cell simulations. It is shown that the two approaches lead essentially to the same results. The unit cell concept has been successfully used for different geometries and applications in CFD modeling in the past [2-5].

In the unit cell approach, the minimum section of regenerator geometry that corresponds to a periodically repeating unit in the flow axial direction as well as the radial direction is specified and modeled. The unit cells thus provide for periodic boundary conditions (BCs) in the axial direction (perpendicular to flow direction) of the regenerator as well as the direction parallel to the flow. Periodic BCs are used to approximate the entire domain by only considering the unit cell. The unit cells will of course include solid material as well as fluid volumes (pores). The solid geometry can be removed from the CFD model, however, and replaced simply with wall BCs.

For periodic boundary conditions at the inlet and outlet, the inlet and outlet faces must be completely matched. As a result, three opposite disks are chosen in a way that the second disk is in the transverse direction of the first disk. Half of the first and third disks, along with the entire thickness of the second disk are included in the unit cell. Figure 2 illustrates the unit cells.

As shown in Figure 2(a), the unit cells that are in the middle of the porous-zone have a θ angle of 45°. The other unit cells at the inner and outer radii of the annular regenerator need to be considered. The θ angles of the inner and outer unit cells are 35.8° and 55.3°, respectively.

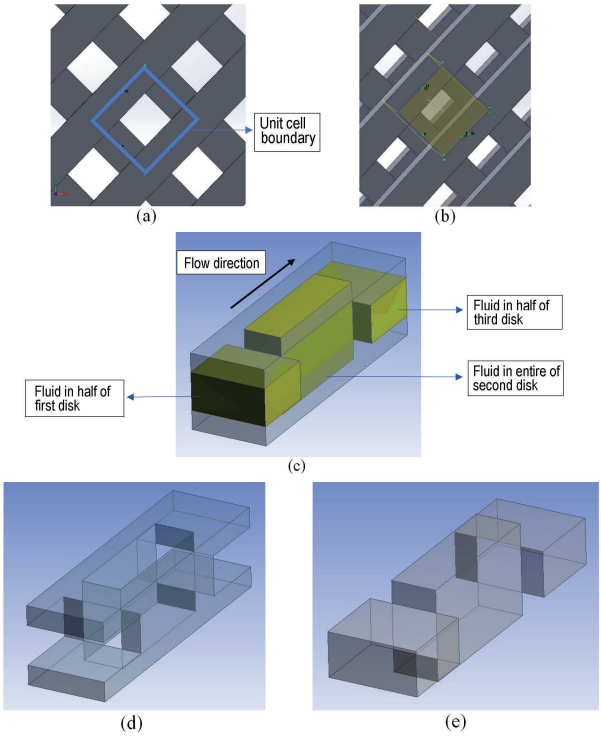

Figure 2. Unit cell selection, (a) cross section of unit cell, (b) 3D unit cell in involute geometry, (c) final unit cell, (d) solid part of unit cell, (e) fluid part of unit cell.

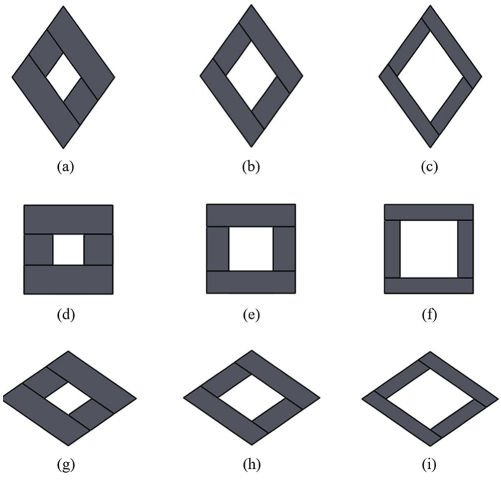

Figure 3. Schematic of different unit cells, (a) θ= 35.8° Φ= 0.35, (b) θ= 35.8° Φ= 0.5, (c) θ= 35.8° Φ= 0.65, (d) θ= 45° Φ= 0.35, (e) θ= 45° Φ= 0.5, (f) θ= 45° Φ= 0.65, (g) θ= 55.3° Φ= 0.35, (h) θ= 55.3° Φ= 0.5, (i) θ= 55.3° Φ= 0.65.

Also, the porosity, referred as Φ, of the baseline model is 0.5. Sensitivity analysis was performed on the porosity of 0.35 and 0.65 of unit cell to find the friction factor and Nusselt number and perform optimization using the Sage computer code [6].

Figure 3 shows the front view of nine different unit cells (only solid part is shown). The hydraulic diameters of the unit cells with porosities of 0.35, 0.5, and 0.65 are 21, 30, and 39 μm, respectively, based on the following definition:

$$D_H = \frac{4V_f}{A_f} \tag{1}$$

where V_f is the fluid volume in the unit cell, and A_f represents the total wetted surface area of the unit cell.

Figure 4 shows the different boundary conditions for a unit cell with a cross angle of 45°, and 0.5 porosity.

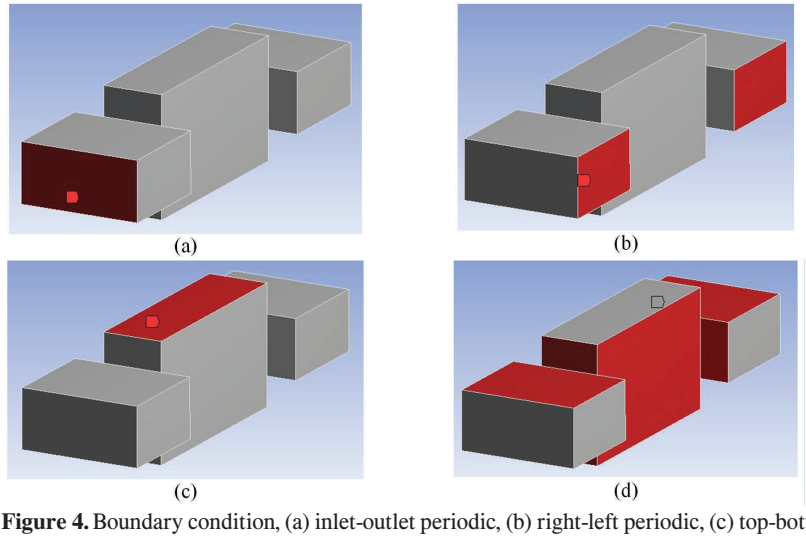

Figure 4. Boundary condition, (a) inlet-outlet periodic, (b) right-left periodic, (c) top-bottom periodic, (d) wall.

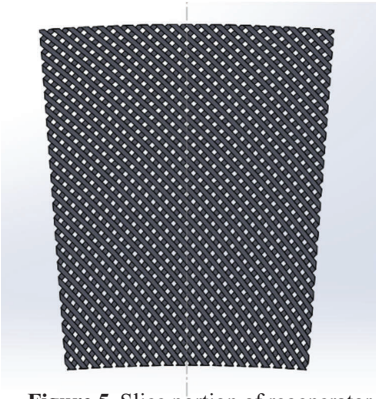

Figure 5. Slice portion of regenerator.

In the disk slice analysis approach, a small slice of the regenerator is chosen as shown in Figure 5. To specify the optimum size of the slice, slices with 2 to 25° were tested by simulation. A 9° slice was found to be the most appropriate because larger angles did not change the simulation results. Since the slice disk is identically repeated in the axial direction, the periodic boundary condition is applied at its front and back faces. Only fluid flow passages are considered in the CFD simulations. The solid body of the regenerator is not included, and all other boundaries are walls.

METHOD OF ANALYSIS

We are interested in developing empirical correlations for friction factor and solid-fluid heat transfer coefficient for the porous structure that can be used with workable volume-averaged conservation equations. This is done by performing detailed pore-level simulations and using the results for deriving volume-average based friction factor and heat transfer coefficients.

The Fanning friction factor is obtained from:

$$f = \frac{\frac{\Delta P}{\Delta x}}{\frac{2}{D_H}\rho_f \langle u \rangle^2} \tag{2}$$

where ρ_f is fluid density, ΔP and Δx represent the pressure drop and axial length associated with the unit cell, respectively, and $\langle u \rangle$ represents the volume-average fluid velocity in a unit cell or disk slice. Microscopic governing equations can be converted to the macroscopic level by the aid of volume averaging [7-9]. The volume average quantities are defined according to

$$\langle \phi \rangle = \frac{1}{V_{CV}} \int_{V_{cv}} \phi \, \mathrm{d}V \tag{3}$$

The Nusselt number is defined according to

$$Nu = \frac{\langle h \rangle D_H}{k_f} \tag{4}$$

where k_f is fluid thermal conductivity and $\langle h \rangle$ represents the local and instantaneous heat transfer coefficient and is calculated as

$$\langle h \rangle = \frac{q''}{\bar{T}_{wall} - \langle T_f \rangle} \tag{5}$$

where q'' is an arbitrary but uniform heat flux applied to all wall boundaries. The quantity $\langle h \rangle$ represents the unit cell or disk slice average heat transfer coefficient. The parameter $\bar{T}_{wall}$ is the

wall average temperature in the unit cell, and (T_f) is the volume-average fluid temperature. These quantities are all found from CFD simulations described later. In the forthcoming analysis and correlations the Reynolds number, defined below, will be used.

$$\mathrm{Re} = \frac{\rho_f \left| \langle \overline{u} \rangle \right| D_H}{\mu_f} \tag{6}$$

where μ_f is the fluid viscosity.

Hexagonal meshes with element sizes of 1 μm and 2 μm tetrahedron elements were used for the unit cell and the disk slice, respectively. The analysis is three-dimensional and steady state. The SIMPLE scheme was used for pressure-velocity coupling to correct the pressure and velocity fields. More details on the numerical formulations can be found in Patankar [10, 11] and Nakayama [12]. The residuals for the continuity and momentum equations in all three Cartesian coordinates were set to 10^{-6}, while the residual for the energy equation was set to 10^{-13}. With appropriate initialization, the simulations converged after around 300 iterations for all of the cases.

RESULTS AND DISCUSSION

The relation between friction factor and Reynolds number can be found by writing

$$f = C_1 + C_2 \mathrm{Re}^m + \frac{C_3}{\mathrm{Re}} \tag{7}$$

where C_1, C_2, m, and C_3 are constants that need to be found from pore-level CFD simulation. With respect to heat transfer, the Nusselt number can be found by curve fitting the pore-level simulation results according to

$$Nu = D_1 + D_2 \mathrm{Re}^k \mathrm{Pr}^n \tag{8}$$

where Pr is the Prandtl number, and D_1, D_2, k, and n are constants.

A least square approach [13] is used for curve fitting and finding aforementioned constants in Equations 7 and 8. Since the flow is laminar, Nu should be a weak function of Re. For thermally-developed laminar flow, the Nusselt number should in fact be independent of Reynolds number.

The figure of merit, which characterizes the performance of regenerators, can be defined as

$$FOM = \frac{Nu}{f\,\mathrm{Re}} \tag{9}$$

Figure 6 compares typical simulation results obtained with the unit cell and disk slice approaches. As noted, the two approaches lead to very similar results and therefore show that the unit-cell based approach, which is far less demanding in terms of computation, is perfectly adequate. Figure 7 compares the simulation results for various unit cells with $\Phi = 0.50$ as well as a disk slice with an angle of 9°, at 300 K temperature. As noted in Table 2 and Figure 6, the friction factor correlations vary slightly with the unit cell type (i.e., the crossing angle), and are independent of temperature. The experimental and computational investigation of Perrella [14, 15] and Pathak [16] also showed that the friction factor in widely-used regenerator fillers is independent of temperature. In practice, however, the difference between unit cell-based and disk slice-based correlations is small (see Figure 7). In fact, using the average friction factor for the three unit cell types will be essentially identical to the disk slice friction factor.

For the current geometry, when the slot crossing angles are not orthogonal, the effective width of the solid webs in the crossing slot direction will get larger as the crossing angle moves further away from 45°. Consequently, flow separation at the entrance and exit will be more severe and therefore the total pressure losses will increase. That is why the effective frictional factor (including form losses) near the inner and outer radii of the annular porous structure will be slightly larger than the midline area.

Table 2 summarizes the results of the simulations where friction factors and Nusselt numbers have been curve-fitted to Equations (7) and (8). Figure 8 shows these curve fittings and CFD data

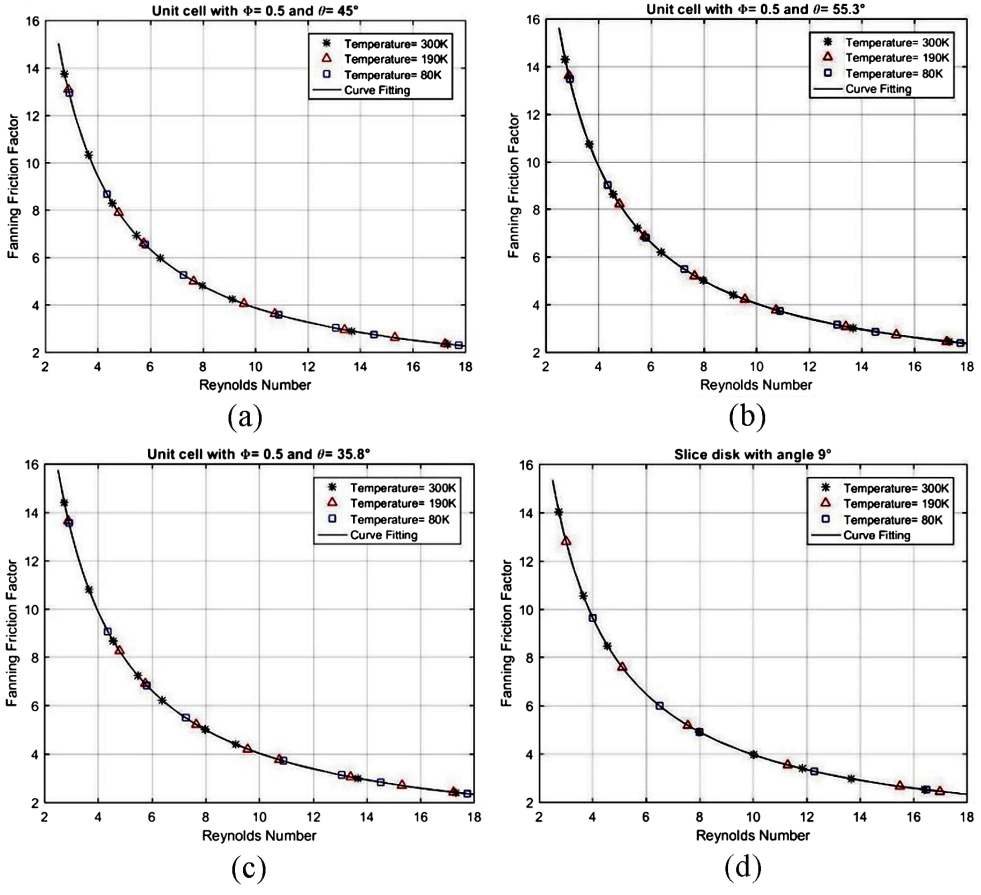

Figure 6. Fanning friction factor versus Reynolds number at different temperatures for unit cells with (a) Φ= 0.50 θ= 45.0°, (b) Φ= 0.50 θ= 45.0°, (c) Φ= 0.50 θ= 35.8°, (d) and slice disk with angle 9°.

Table 2. Fanning friction factor correlations for Re range 2-18, average Nusselt numbers, and figure of merits at Re= 10.

Unit cell	$f = C_1 + C_2\,\mathrm{Re}^m + \frac{C_3}{\mathrm{Re}}$				$Nu = D_1$	$FOM = \frac{Nu}{f\,\mathrm{Re}}$
Porosity & Crossing angle	C_1	C_2	C_3	m	D_1	
Φ= 0.35, θ= 35.8°	0	0.095	40.503	0.522	7.220	0.165
Φ= 0.35, θ= 45.0°	0	0.094	39.798	0.516	7.356	0.171
Φ= 0.35, θ= 55.3°	0	0.096	40.533	0.520	7.222	0.165
Φ= 0.50, θ= 35.8°	0	0.035	39.198	0.499	8.226	0.204
Φ= 0.50, θ= 45.0°	0	0.043	37.372	0.512	8.382	0.216
Φ= 0.50, θ= 55.3°	0	0.050	38.858	0.479	8.224	0.204
Disk slice	0	0.048	38.180	0.509	8.333	0.210
Φ= 0.65, θ= 35.8°	0	0.019	34.832	0.562	9.221	0.259
Φ= 0.65, θ= 45.0°	0	0.016	34.753	0.604	9.221	0.260
Φ= 0.65, θ= 55.3°	0	0.016	34.820	0.616	9.221	0.259

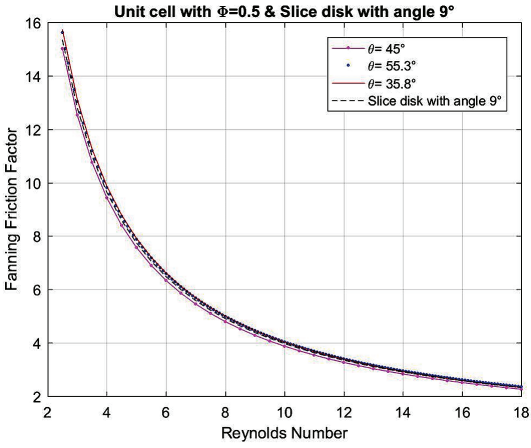

Figure 7. Fanning friction factor versus Reynolds number for different unit cells with Φ=0.50 and slice disk with angle 9°.

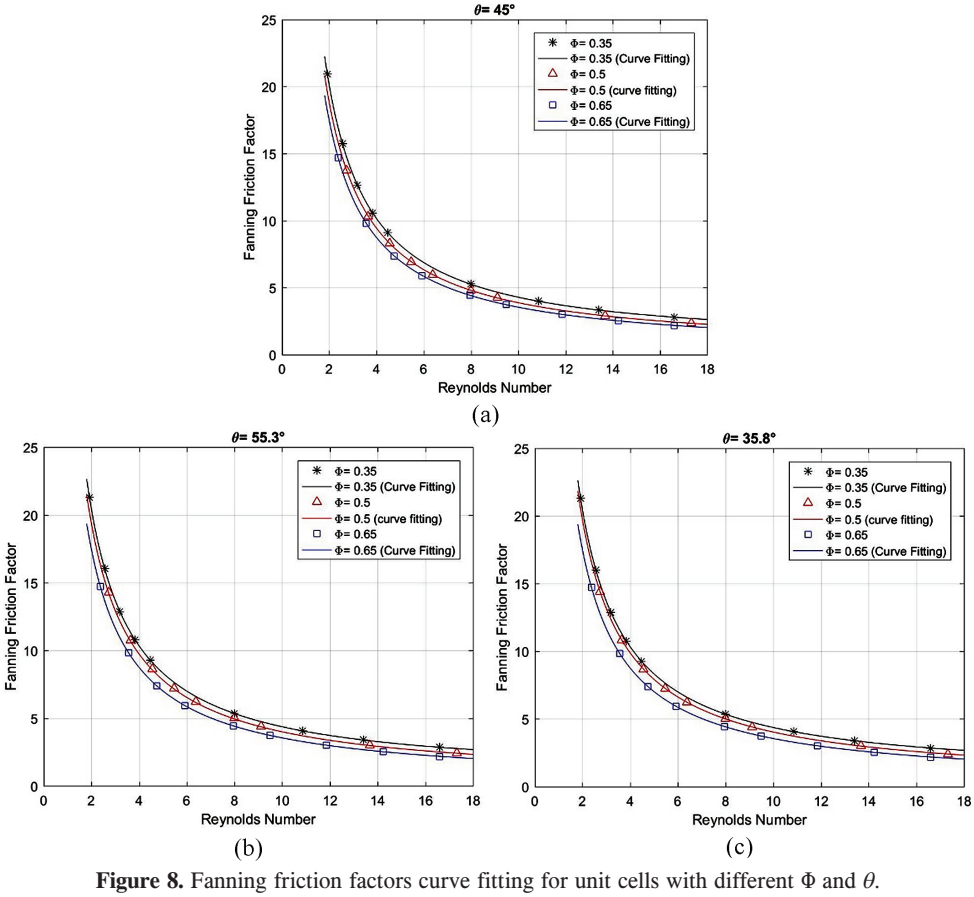

Figure 8. Fanning friction factors curve fitting for unit cells with different Φ and θ.

points results at different Reynolds numbers. Table 2 represents results of Nusselt numbers for Re= 10. Simulations with Re= 5 produced exactly the same results, confirming the expected constant *Nu* number.

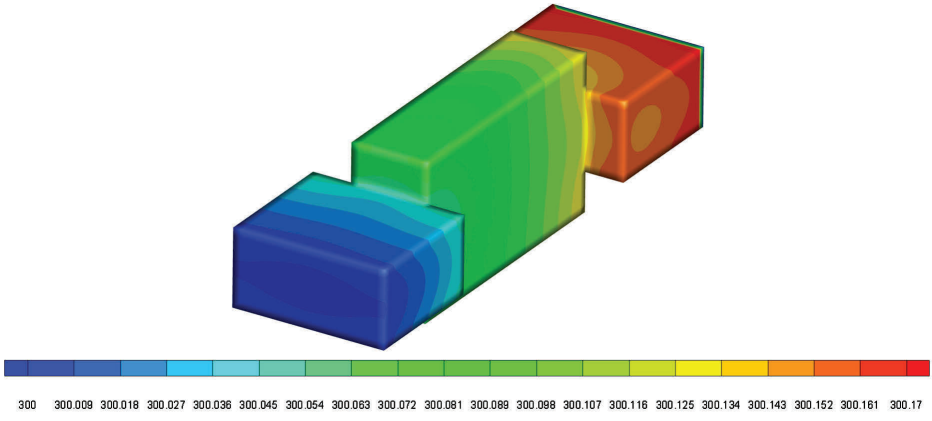

Figure 9. Temperature distribution (in Kelvin) after applying arbitrary heat flux, here 300 W/m^2, from the walls in a single unit cell.

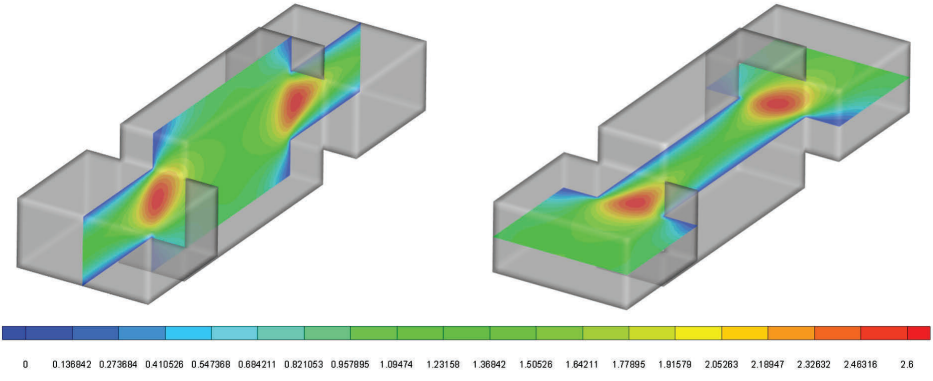

Figure 10. Velocity distributions (in m/s) in a single unit cell.

Figures 9 and 10 shows typical temperature distributions and velocity profiles in a unit cell with $\Phi = 0.50$, $\theta = 45.0^\circ$ respectively. The complex geometry of the flow passage leads to the formation of recirculation cells that in turn lead to irreversibility and entropy generation, which will be investigated in the future.

The figure of merit, predicted by simulations, could be correlated as,

$$FOM_{slice} = \frac{8.333}{0.048\,\mathrm{Re}^{1.509} + 38.180} \tag{10}$$

FOM depends on Re only slightly. $FOM_{slice} = 0.21$ for Re = 10, and is higher than stacked screens and packed sphere beds for which *FOM* is typically lower than 0.1. This value increases as the porosity increases and eventually will approach that of parallel plates, which is about 0.32.

CONCLUSIONS

A methodology for the prediction and correlation of friction and heat transfer in a novel, micro-structured regenerator filler was described in this paper. Using detailed pore-scale CFD simulations, empirical correlations were derived for the friction factor and solid-fluid heat transfer coefficient (Nusselt number). Pore-level analysis was done for single unit cells as well as disk slices that contained a large number of unit cells. The derived empirical correlations can be used in CFD simulations when the regenerator is modeled as a porous medium.

ACKNOWLEDGMENT

This study was funded by the Georgia Tech Foundation through a research grant provided by West Coast Solutions.

REFERENCES

1. ANSYS, ANSYS FLUENT User's Guide. No. Release 14.5, Canonsburg, PA 15317: Southpointe, (2012).
2. Pathak, M.G., Mulcahey, T.I. and Ghiaasiaan, S.M., "Conjugate heat transfer during oscillatory laminar flow in porous media," *International Journal of Heat and Mass Transfer*, *66*, (2013), pp. 23-30.
3. Fumoto, Y., Liu, R., Sano, Y. and Huang, X., "A three-dimensional numerical model for determining the pressure drops in porous media consisting of obstacles of different sizes," *The Open Transport Phenomena Journal*, *4*, (2012), pp. 1-8.
4. Coulaud, O., Morel, P. and Caltagirone, J.P., "Numerical modelling of nonlinear effects in laminar flow through a porous medium," *Journal of Fluid Mechanics*, *190*, (1988), pp. 393-407.
5. Nakayama, A., Kuwahara, F., Umemoto, T. and Hayashi, T., "Heat and fluid flow within an anisotropic porous medium," *Journal of heat transfer*, *124*, no. 4 (2002), pp. 746-753.
6. Gedeon, D., Sage User's Guide, Sage v11 Edition, 259 (2016).
7. Whitaker, S., *The method of Volume Averaging. Theory and Applications of Transport in Porous Media*, Kluwer Academic Publishers, (1999).
8. Ochoa-Tapia, J. A., and Whitaker, S., "Momentum transfer at the boundary between a porous medium and a homogeneous fluid—I. Theoretical development," *International Journal of Heat and Mass Transfer*, *38*(14), (1995), pp. 2635-2646.
9. Ochoa-Tapia, J. A., and Whitaker, S., "Heat transfer at the boundary between a porous medium and a homogeneous fluid," *Int. Journal of Heat and Mass Transfer*, *40*(11), (1997), pp .2691-2707.
10. Patankar, S. V., and Spalding, D.B., "A calculation procedure for heat, mass and momentum transfer in three-dimensional parabolic flows," *International Journal of Heat and Mass Transfer,* vol. 15, (1972), pp. 1787-1806.
11. Patankar, S. V., *Numerical heat transfer and fluid flow*, CRC press, (1980).
12. Nakayama, A., *PC-aided numerical heat transfer and convective flow*, CRC press, (1995).
13. Chapra, S.C. and Canale, R.P., *Numerical methods for engineers*, Vol. 2, McGraw-Hill, New York (1998).
14. Perrella, M. D., and S. M. Ghiaasiaan, "Periodic flow hydrodynamic resistance parameters for woven screen matrices at cryogenic temperatures," *IOP Conference Series: Materials Science and Engineering*. Vol. 278. No. 1. IOP Publishing, (2017).
15. Perrella, M. D., *Periodic Flow Hydrodynamic Resistance parameters for Microporous Cryocooler Regenerator Filler materials at Cryogenic Temperatures,* PhD Thesis, Georgia Institute of Technology (2016).
16. Pathak, M. G., et al., "Hydrodynamic resistance parameters for ErPr rare-earth regenerator material under steady and periodic flow conditions," *AIP Conference Proceedings*. Vol. 1573. No. 1. AIP, (2014).